第 33 卷第 11 期
2017 年 11 月

无 机 化 学 学 报
CHINESE JOURNAL OF INORGANIC CHEMISTRY

Vol.33 No.11
2045-2050

基于 π-共轭 4-四硫富瓦烯-2,6-吡嗪吡啶配体的 Fe(Ⅱ)配合物

谢家泽[1] 王大鹏[1] 马建平[2] 王海英*,[1,3] 左景林[1]

([1]南京大学化学化工学院,配位化学国家重点实验室,人工微结构科学与技术协同创新中心,南京 210093)

([2]山东师范大学化学化工与材料科学学院,济南 250014)

([3]山东科技大学化学与环境工程学院,青岛 266590)

摘要:设计、合成了功能化的 4-四硫富瓦烯-2,6-吡嗪吡啶配体(L),并以此为配体合成了具有电活性的配合物$[Fe(Ⅱ)(L)_2](BF_4)_2\cdot 2.75CH_3CN\cdot 0.25CH_2Cl_2$ (**1**),通过红外、元素分析及 X 射线单晶衍射等手段对所合成的化合物进行了表征。配体以三齿的方式参与配位,形成离散型的配合物 **1**,该配合物中含有多种非经典氢键和 π…π 以及 S…S 作用。此外研究了该配合物的磁性、电化学性质和光谱电化学性质。

关键词:四硫富瓦烯;Fe(Ⅱ)配合物;多功能材料;晶体结构

中图分类号:O614.81+1 **文献标识码**:A **文章编号**:1001-4861(2017)11-2045-06

DOI:10.11862/CJIC.2017.246

Iron(Ⅱ) Complex Based on π-Conjugated 4-Tetrathiafulvalene-2,6-di(pyrazin-2-yl)pyridine Ligand

XIE Jia-Ze[1] WANG Da-Peng[1] MA Jian-Ping[2] WANG Hai-Ying*,[1,3] ZUO Jing-Lin[1]

([1]*State Key Laboratory of Coordination Chemistry, School of Chemistry and Chemical Engineering, Collaborative Innovation Center of Advanced Microstructures, Nanjing University, Nanjing* 210023, *China*)

([2]*School of Chemistry, Chemical Engineering and Materials Science, Shandong Normal University, Jinan* 250014, *China*)

([3]*College of Chemical and Environmental Engineering, Shandong University of Science and Technology, Qingdao, Shandong* 266590, *China*)

Abstract: The tetrathiafulvalene (TTF) functionalized 2,6-di(pyrazin-2-yl)pyridine derivative, 4-tetrathiafulvalene-2,6-di(pyrazin-2-yl)pyridine (L), was designed and synthesized. Based on L, one electrochemically active TTF-containing Fe(Ⅱ) complex, namely, $[Fe(Ⅱ)(L)_2](BF_4)_2\cdot 2.75CH_3CN\cdot 0.25CH_2Cl_2$ (**1**), was synthesized and characterized by IR, elemental analysis, and X-ray single crystal diffraction. The complex **1** is formed by ligands and iron(Ⅱ) in a tridentate fashion. Complex **1** exhibits a discrete structure and features diverse nonclassical hydrogen bonding interactions, π…π and S…S interactions. In addition, magnetic, electrochemical, and spectroelectrochemistry properties for complex **1** have been studied. CCDC: 1565586.

Keywords: tetrathiafulvalene; Fe(Ⅱ) complex; multifunctional materials; crystal structure

In recent years, the design and study of multifunctional molecule-based magnetic materials has attracted enormous attention owing to their potential applications across a plethora of areas such as in molecular spintronics, and new bifunctional materials[1-2]. Meanwhile, the exquisite control that can be

收稿日期:2017-08-01。收修改稿日期:2017-09-18。

科技部国家重大科学研究计划(No.2013CB922101)、国家自然科学基金(No.91433113,91422302)和江苏省自然科学基金(No.BK20130054)资助项目。

*通信联系人。E-mail:haiyingqd@163.com

achieved over the design of coordination compounds via rational structural modifications to the component metal ions and ligands provides unique prospects for designing structures and elucidating fundamental structure-function relationship[3-5]. Tetrathiafulvalene (TTF) and its derivatives, known as π-electron donors capable of forming stable cation radical and dication species upon oxidation, can be used to construct novel functional materials as versatile building blocks due to its unique structural and electronic diversities[6-8]. The incorporation of magnetic moment carriers such as Fe(Ⅱ) and Co(Ⅱ) ions into coordination compounds allows for the development of novel multifunctional materials with additional magnetic properties, including ferromagnetism or ferrimagnetism, and spin crossover behavior, which has exceptional potential in technological applications such as data storage and display devices[9-10]. Recently, several Fe(Ⅱ) coordination compounds based on the terpyridine-tetrathiafulvalene (TTF-terpy) have been studied[11]. These compounds retain the redox activity of the TTF moiety and moreover some exhibit antiferromagnetic interactions arising from Fe(Ⅱ) ions.

In this paper, we design a new π-extended ligand consisting of pyrazinyl and pyridine moiety and redox-active TTF core. Based on this novel functional ligand, an iron complex, $[Fe(Ⅱ)(L)_2](BF_4)_2\cdot 2.75CH_3CN\cdot 0.25CH_2Cl_2$ (**1**), is successfully synthesized and the crystal structure is obtained. Its Magnetic, electrochemical and UV-Vis properties were studied.

1 Experimental

1.1 Materials and instruments

All reagents and solvents were obtained from commercial sources and used without further purification.

IR spectra were recorded in range of 400~4 000 cm^{-1} on a Vector27 Bruker Spectrophotometer with KBr pellets. C, H, N and S analyses were carried out on a Perkin-Elmer 240C analyzer. Mass spectra were determined on a Varian MAT 311A instrument for ESI-MS. Magnetic susceptibility measurements were performed using a Quantum Design SQUID VSM magnetometer on the crystalline sample for complex **1**. Cyclic voltammetry measurements were performed in n-Bu_4NPF_6/CH_3CN electrolyte using a BAS Epsilon electrochemical analyser and three electrode system. All potentials are reported in mV versus Fc/Fc^+ couple. Absorption spectra were measured on a UV-3100 spectrophotometer.

1.2 Synthesis of the ligand L

1.2.1 Synthesis of the formyltetrathiafulvalene (TTF-CHO)

To a mixture of TTF (696 mg, 3.4 mmol) in anhydrous ether (60 mL) was added lithium diisopropylamide (LDA, 2.6 mL, 2.0 $mol\cdot L^{-1}$ solution in THF) under nitrogen at −78 ℃. After the mixture was stirred for 2 h, Ph(Me)NCHO (1.04 mL) was added dropwise. The mixture was stirred at −78 ℃ for 1 h and then for 12 h at room temperature. Under N_2 protection, hydrochloric acid (15 mL, 1 $mol\cdot L^{-1}$) was added and the reactant was stirred for 20 min to quench the reaction. The aqueous phase was extracted with dichloromethane (60 mL×3), and the organic extracts were washed with brine, dried over sodium sulfate, filtered, and concentrated. The residue was purified by a silica column using dichloromethane/petroleum ether as an eluent to afford TTF-CHO as a dark red solid (Yield: 58.8%).

1.2.2 Synthesis of the ligand L

A mixture of TTF-CHO (463.8 mg, 2 mmol) in

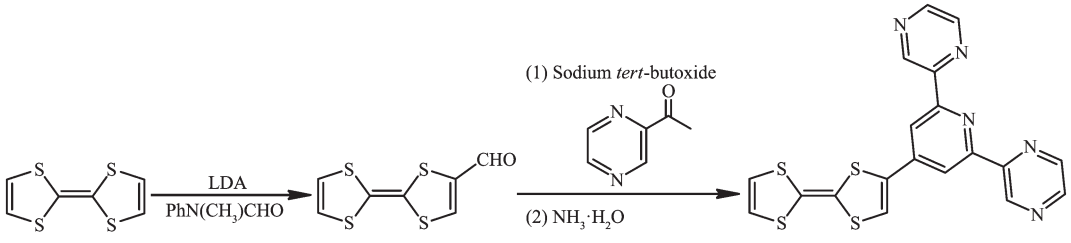

Scheme 1 Synthesis of ligand L

THF (30 mL), 2-acetylpyridine (488.2 mg, 4 mmol) in ethanol (15 mL), and *t*-BuONa (528.6 mg, 5.5 mmol) in ethanol (15 mL) under nitrogen was stirred at room temperature for 0.5 h. After adding concentrated ammonia (7.2 mL), the reaction mixture was stirred for 20 h. After filtration, the resulting residue was washed several times with methanol and dried by vacuum. The resulting ligand L was obtained as a dark red solid in 20.6% yield. Anal. Calcd. for $C_{19}H_{11}N_5S_4$(%): C, 52.15; H, 2.53; N, 16.01; S, 29.31. Found(%): C, 52.11; H, 2.55; N, 15.97; S, 29.30. IR (KBr, cm^{-1}): 3 408m, 3 065w, 1 611m, 1 533m, 1 466w, 1 425w, 1 401 w, 1 328s, 1 261m, 1 219m, 1 192m, 1 034s, 848w, 800m, 732w, 685w, 634w, 525w, 448w. MS (*m/z*): Calcd. for $C_{19}H_{11}N_5S_4$ (M^+) 436.99; Found 437.42.

1.3 Synthesis of 1

Under nitrogen, to the CH_2Cl_2 solution of L (0.02 $mol\cdot L^{-1}$, 10 mL) was added $Fe(BF_4)_2\cdot 6H_2O$ (33.8 mg, 0.1 mmol) and a few grains of ascorbic acid in CH_3OH (10 mL). The reaction mixture was stirred under reflux for 20 h. After filtration, the resulting residue was washed several times with methanol, dried by vacuum and recrystallized from 80 mL acetonitrile. The resulting complex **1** was obtained as a dark blue solid in 43.5% yield. Crystals of **1** were grown by slow diffusion of diethyl ether into an acetonitrile solution of **1** at −6 ℃. Anal. Calcd. for $C_{43.5}H_{30.75}B_2Cl_{0.50}F_8FeN_{12.75}S_8$(%): C, 42.28; H, 2.51; N, 14.45; S, 20.76. Found (%): C, 42.25; H, 2.48; N, 14.50; S, 20.72. IR (KBr, cm^{-1}): 3 408m, 3 065w, 1 611m, 1 533w, 1 466w, 1 425 w, 1 401w, 1 328s, 1 261m, 1 219w, 1 192m, 1 034s, 848w, 800m, 732w, 685w, 634w, 522w, 448w.

1.4 Crystal structure determination

The crystal data were collected with Mo $K\alpha$ radiation (λ=0.071 073 nm) on a CCD diffractometer. The cell parameters were retrieved and refined by using computer software (SMART and SAINT, respectively)[12]. The SADABS[13] program was applied for absorption corrections. Structure was solved by direct methods using the program package SHELXL-97[14]. All the non-hydrogen atoms were located in the Fourier maps and refined with anisotropic parameters. Crystallographic data are summarized in Table 1. Selected bond lengths (nm) and bond angles (°) are listed in Table 2.

CCDC: 1565586.

Table 1　Crystallographic data of complex 1

Formula	$C_{43.5}H_{30.75}B_2Cl_{0.50}F_8FeN_{12.75}S_8$	Temperature / K	296(2)
Formula weight	1 238.74	*Z*	2
Crystal system	Triclinic	D_c / ($g\cdot cm^{-3}$)	1.501
Space group	$P\bar{1}$	Size / mm	0.23×0.16×0.09
a / nm	1.358 8(3)	*F*(000)	1 254
b / nm	1.480 0(4)	Absorption coefficient / mm^{-1}	0.677
c / nm	1.603 0(4)	Reflection collected, used	16 111, 1 064
α / (°)	110.446(4)	Independent reflection (R_{int})	10 340(0.078 7)
β / (°)	91.895(4)	Goodness-of-fit on F^2	1.027
γ / (°)	112.379(4)	θ range for data collection / (°)	1.62~25.68
V / nm^3	2 741.4(12)	R_1, wR_2 [$I>2\sigma(I)$]	0.091 8, 0.238 6

Table 2　Selected bond lengths (nm) and bond angles (°) of the complex 1

Fe(1)-N(2)	0.198 3(7)	Fe(1)-N(4)	0.196 7(7)	Fe(1)-N(8)	0.186 7(7)
Fe(1)-N(3)	0.187 8(7)	Fe(1)-N(7)	0.195 9(7)	Fe(1)-N(9)	0.194 7(7)
N(3)-Fe(1)-N(2)	80.8(3)	N(3)-Fe(1)-N(9)	98.1(3)	N(7)-Fe(1)-N(4)	90.7(3)
N(3)-Fe(1)-N(4)	80.6(3)	N(4)-Fe(1)-N(2)	161.3(3)	N(8)-Fe(1)-N(2)	98.4(3)
N(3)-Fe(1)-N(7)	99.4(3)	N(7)-Fe(1)-N(2)	91.4(3)	N(8)-Fe(1)-N(3)	178.6(3)
N(8)-Fe(1)-N(4)	100.3(3)	N(8)-Fe(1)-N(7)	81.7(3)	N(8)-Fe(1)-N(9)	80.8(3)
N(9)-Fe(1)-N(2)	92.9(3)	N(9)-Fe(1)-N(4)	90.6(3)	N(9)-Fe(1)-N(7)	162.4(3)

2 Results and discussion

2.1 Crystal structure

The ORTEP diagram of the complex **1** is depicted in Fig.1. The crystal structure of **1** adopts the triclinic system (space group $P\bar{1}$), and the asymmetric unit contains one $[Fe(Ⅱ)(L)_2]^{2+}$ cation, two BF_4^- anions, a quarter CH_2Cl_2 molecule and 2.75 CH_3CN molecules. In each $[Fe(Ⅱ)(L)_2]^{2+}$ cation, the central iron(Ⅱ) ion lies on the inversion center and adopts a distorted $[FeN_6]$ octahedral coordination environment, which is defined by two nitrogen donors from four pyrazine nitrogen donors and two pyridyl nitrogen donors from two ligands. The Fe-N bonds range from 0.186 7(4) to 0.198 3(7) nm suggesting that the Fe1 ions are in low-spin (LS) states at 296 K[15]. The TTF moieties of the two L ligands all adopt a U-like configuration with a dihedral angle 13.6°, 6.2°, 8.1° and 25.3° folding at S1 -S2, S3-S4, S5-S6, and S7-S8, respectively. The central C=C bond length of the TTF cores are 0.130 0(13) nm for C3-C4 and 0.127 8(13) nm for C22-C23. The bond lengths and angles are close to those reported for the neutral unit[16], indicating that the ligand can still be regarded as charge neutral. Complex **1** stacks together to give a two-dimensional (2D) network through nonclassical hydrogen bonds C(11)–H(11)⋯F(3), C(21)–H(21)⋯F(2), C(32)–H(32)⋯F(6)^{i}, C(33)–H(33)⋯F(4), and C(30)–H(30) ⋯F(5) ($d_{H\cdots F}$=0.246, 0.240, 0.240, 0.231 and 0.237 nm, respectively. Symmetry codes: ^{i}2–x, 1–y, 2–z) (Fig.2a). Through nonclassical hydrogen bonds (C(19)–H(19)⋯F(3), $d_{H\cdots F}$=0.246 nm; C(39)–H(39)^{ii}⋯F(6), $d_{H\cdots F}$=0.242 nm), the solvent CH_3CN molecules are connected to the 2D network. Intermolecular $\pi\cdots\pi$ contacts were found (Fig.2b). The C⋯C distances between two neighboring TTF cores are 0.365 2 and 0.376 8 nm and the distances of pyrazine units are 0.372 6 and 0.383 7 nm. In addition, weak S⋯S interactions (<0.370 nm) can be observed in the packing diagram[17]. The shortest S⋯S distance between two neighboring TTF cores is 0.368 4 nm.

2.2 Magnetic properties

Variable-temperature (T) magnetic susceptibility ($\chi_M T$) measurements were performed on the sample of complex **1** in the range of 2~300 K. At room temperature, most of the Fe(Ⅱ) ions are in LS states. As shown in Fig.3, the $\chi_M T$ value is 0.57 $cm^3\cdot mol^{-1}\cdot K$ at 300 K[18]. As the temperature decreases, the $\chi_M T$ value gradually drops close to zero at 2.0 K due to the remain high-spin (HS) Fe(Ⅱ) gradually turned to LS, which indi-

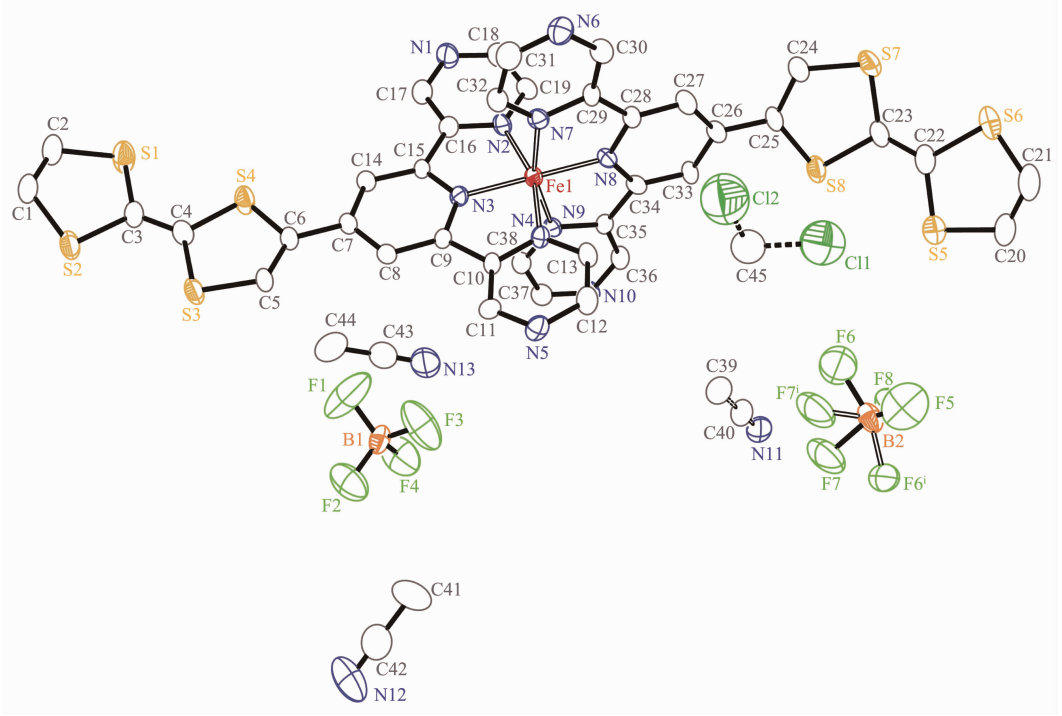

Symmetry codes: ^{i} 2–x, 1–y, 2–z

Fig.1 Structure of the complex **1**

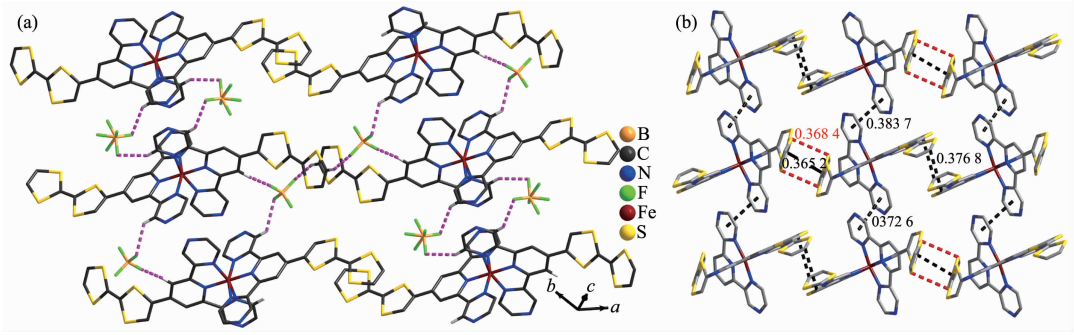

Fig.2　Crystal-packing arrangement of **1** showing nonclassical hydrogen bonding interactions (a), π···π (black line) and S···S (red dashed line) interactions (b)

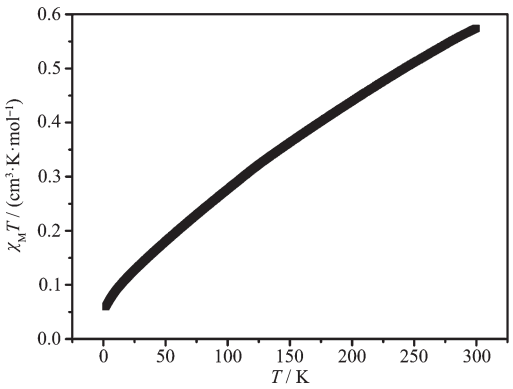

Fig.3　Temperature dependence of $\chi_M T$ for complex **1** at 1 kOe

cates an gradually SCO transition[19].

2.3　Solution-State electrochemistry

Solution-state electrochemistry was performed on L and complex **1**. The electrochemical property for L was investigated by using cyclic voltammetry (CV) in DMF (0.1 mol·L^{-1} n-Bu_4NClO_4). For complex **1**, cyclic voltammetry (CV) and differential pulse voltammetry (DPV) were used in CH_3CN (0.1 mol·L^{-1} n-Bu_4NClO_4). As shown in Fig.4, two reversible oxidation couples were observed at $E_{1/2}$=0.09 and 0.31 V for L, which are associated with the successive oxidation of neutral TTF (TTF^0) to the radical cation (·TTF^+) and then to the dication (TTF^{2+}). Upon coordination, the CV of **1** shows three distinct redox processes. The two reversible redox peaks at $E_{1/2}$=0.18 V and 0.53 V can be assigned to the TTF/·TTF^+ and ·TTF^+/TTF^{2+} redox couples, respectively. The third redox peak at $E_{1/2}$= 1.44 V can be assigned to the Fe(Ⅲ)-centered one-electron oxidation process. Three peaks of DPV correspond to the redox processes of CV, and the ratio of integral area for three peaks is 2∶2∶1 (the ratio of TTF moieties to Fe(Ⅱ) per complex molecule is 2∶1), which suggests that the three-step redox process is independent single-electron transfer process.

2.4　Spectroelectrochemistry

Given the nature of CV, solution-state spectroelectrochemical measurements were conducted to gain

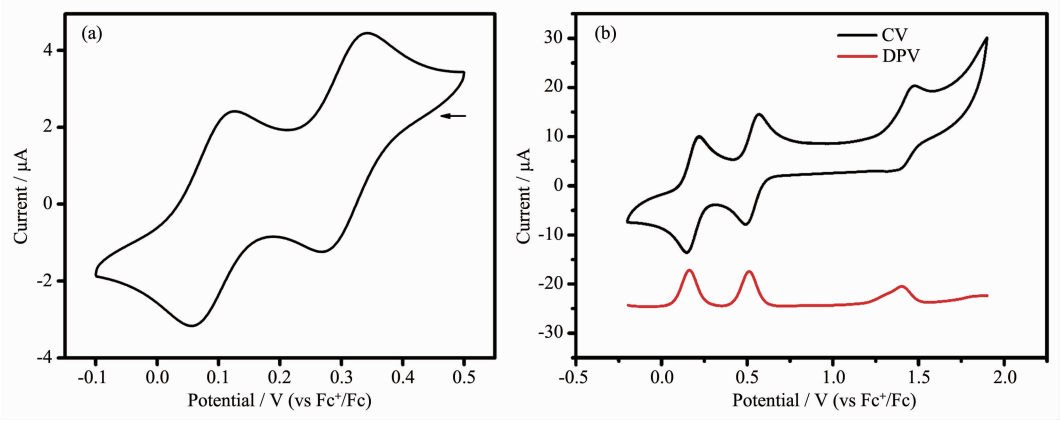

Range: −0.1~0.5 V for L, −0.2~1.9 V for complex **1**; Arrow indicates the direction of the forward scan

Fig.4　Solution-state electrochemistry of L (a) and complex **1** (b)

insight into the origins of the electrochemical processes for **1** (Fig.5a). The measurements were also carried out during the electrolysis of the solution of complex **1** in CH_3CN at suitable constant potentials corresponding to its redox processes. Upon increasing the applied potential from 0 to 0.45 V, the bands at 466 nm increases due to formation of the $\cdot TTF^+$ radical cation. Upon increasing the potential from 0.5 to 0.7 V, the electronic spectra show a decrease in the characteristic absorptions of the radical cation bands due to formation of TTF^{2+} dication (Fig.5b).

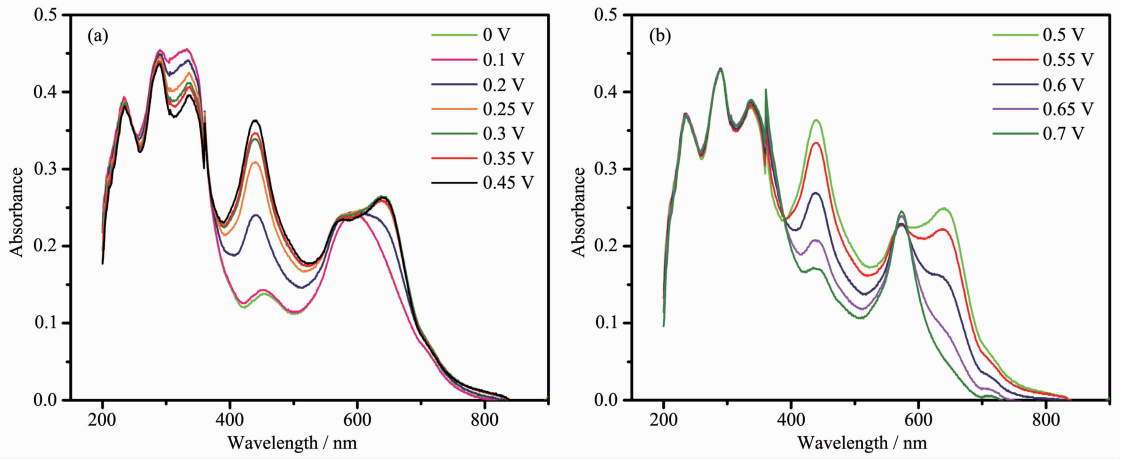

Fig.5 Spectroelectrochemistry on **1** over the potential range of 0~0.45 V (a) and 0.5~0.7 V (b)

3 Conclusions

One discrete complex based on the redox-active 4-tetrathiafulvalene-2,6-di(pyrazin-2-yl)pyridine ligand was synthesized and structurally characterized. At room temperature, most of the Fe(Ⅱ) ions are in LS states. Complex **1** features diverse nonclassical hydrogen bonding interactions, $\pi \cdots \pi$ and S ⋯ S interactions. The interesting redox activity for complex **1** has been probed via solution-state electrochemistry, revealing multiple processes due to the redox properties of both the TTF and metal ions. The results suggest that the incorporation of redox-active ligands into complexes can be useful for the development of interesting redox-active materials. Further investigations on TTF compounds with new structures and multifunctional properties are ongoing in our group.

References:

[1] Mannini M, Pineider F, Danieli C, et al. *Nature*, **2010**,**468**(7322):417-421

[2] Bogani L, Wernsdorfer W. *Nat. Mater.*, **2008**,**7**(3):179-186

[3] Wang G, Xue Z, Pan J, et al. *CrystEngComm*, **2016**,**18**(43):8362-8365

[4] Ma J P, Zhao C W, Wang S Q, et al. *Chem. Commun.*, **2015**,**51**(78):14586-14589

[5] Ma J P, Wang S Q, Zhao C W, et al. *Chem. Mater.*, **2015**,**27**(11):3805-3808

[6] Wang H Y, Cui L, Xie J Z, et al. *Coord. Chem. Rev.*, **2017**,**345**:342-361

[7] Cui L, Zhu F, Leong C F, et al. *Sci. China Ser. B: Chem.*, **2015**,**58**(4):650-657

[8] Yao M, Zheng Q, Gao F, et al. *Sci. China Ser. B: Chem.*, **2012**,**55**(6):1022-1030

[9] Bousseksou A, Molnar G, Salmon L, et al. *Chem. Soc. Rev.*, **2011**,**40**(6):3313-3335

[10]Pointillart F, Liu X, Kepenekian M, et al. *Dalton Trans.*, **2016**,**45**(28):11267-11271

[11]Hu L, Liu W, Li C H, et al. *Eur. J. Inorg. Chem.*, **2013**,**2013**(35):6037-6048

[12]*SAINT-Plus, Version* 6.02, Bruker Analytical X-ray System, Madison, WI, **1999**.

[13]Sheldrick G M. *SADABS: An Empirical Absorption Correction Program*, Bruker Analytical X-ray Systems, Madison, WI, **1996**.

[14]Sheldrick G M. *Acta Crystallogr. Sect. A: Found. Crystallogr.*, **2008**,**A64**:112-122

[15]Liu W T, Li J Y, Ni Z P, et al. *Cryst. Growth Des.*, **2012**,**12**(3):1482-1488

[16]Iwahori F, Golhen S, Ouahab L, et al. *Inorg. Chem.*, **2001**,**40**(26):6541-6542

[17]Nishikawa H, Kitabatake R, Mitsumoto K, et al. *Crystals*, **2012**,**2**:935-945

[18]Shatruk M, Dragulescu-Andrasi A, Chambers K E, et al. *J. Am. Chem. Soc.*, **2007**,**129**(19):6104-6116

[19]Seredyuk M, Piñeiro-López L, Muñoz M C, et al. *Inorg. Chem.*, **2015**,**54**(15):7424-7432